Microalloying Effect on the Precipitation Processes of Mg-Ca Alloys

CHAMINI L. MENDIS, KEIICHIRO OH-ISHI, and KAZUHIRO HONO

The Mg-Ca binary alloys in the Mg-Mg_2Ca two-phase region show little precipitation hardening by aging. However, the Mg-Ca alloys microalloyed with Al and Zn result in notable age hardening because of the formation of metastable, internally ordered, plate-like Guinier–Preston (GP) zones on the basal plane. To enhance the age-hardening response, we explored microalloying elements that can alter the habit plane from basal to prismatic. We found that an indium addition causes the homogeneous precipitation of thin plates on prismatic planes, resulting in a pronounced age-hardening response. Based on transmission electron microscopy and atom probe analysis results, we discuss the structure of the GP zones and the possible origin of the habit plane alternation.

DOI: 10.1007/s11661-011-1049-5
© The Minerals, Metals & Materials Society and ASM International 2012

I. INTRODUCTION

BEING the lightest of all structural metals, magnesium alloys have the potential to replace conventional structural materials in certain applications where weight reduction is critical. However, only cast alloys are currently used in limited applications such as engine blocks, and no wrought products are used as structural components in transportation vehicles because magnesium alloys lack sufficient formability, strength, ductility, and corrosion resistance. When energy efficiency becomes more important than materials' cost in transportation vehicles in the future, it might be possible to use wrought magnesium alloys as substitutes for some existing structural materials. For wider applications of wrought magnesium alloys, it is essential to develop higher strength wrought alloys. One way to achieve this is to develop age-hardenable alloys that can be solution treated before wrought processes, and then the strength of final products can be enhanced by short heat treatments.[1]

In our previous studies,[2–4] we reported that minor additions of Ag + Ca substantially enhance the age-hardening response of the Mg-Zn alloy, which is attributed to the refinement of $MgZn_2$ (β_1') precipitates.[2] The wrought alloys developed based on this system, Mg-2.4 Zn-0.1Ag-0.1Ca-0.16Zr (ZQXK), show a yield strength of 325 MPa with an elongation of 14 pct after a T6 heat treatment.[3,4] The fine precipitates that form dynamically during the extrusion process pin the grain boundaries to refine the recrystallized grain size after the wrought process, and the T6 heat treatment induces the dispersion of nanosized precipitates within the grains, which increases the yield strength to more than 300 MPa. A similar microstructure development has also been reported in Mg-Sn alloy microalloyed with Zn and Al.[5] These investigations suggest that the search for microalloying elements to base binary two-phase alloy is an effective way to develop new age-hardenable wrought alloys.

The equilibrium phase diagram of the Mg-Ca system indicates that an α + Mg_2Ca two-phase region exists.[6] Because the melting point of the Mg_2Ca phase is ~711 °C,[6] the alloys containing Mg_2Ca may be a potential creep-resistant alloy.[7] Thus, in this article, we focus on the precipitation process of Mg-Ca based alloys. The age-hardening response of binary Mg-Ca alloys is almost nil because of a sluggish precipitation of coarse equilibrium Mg_2Ca phase.[8] However, microalloying with Al, Zn, and In causes the precipitation of metastable plate-like precipitates with a high number density in a relatively short time. In particular, we found that the addition of In alters the habit plane of the precipitates from the basal plane to the prismatic planes. In this article, we review the effect of these microalloying effects on the precipitation processes of Mg-Ca based alloy and discuss the possibility of developing new age-hardenable, high-strength Mg-Ca based alloys.

II. MICROALLOYING EFFECT OF ZN AND AL

The age-hardening curves of Mg-0.3Ca-0.6Zn and Mg-0.3Ca-0.3Al alloys are shown in Figure 1 together with that of the Mg-0.3Ca alloy. The alloys were solution heat treated at 798 K (525 °C) for 1 hour, and then were quenched to iced brine and aged at 473 K (200 °C). Although the binary alloy shows a minor age hardening, the Mg-Ca alloy microalloyed with 0.6 at. pct Zn shows a rapid increase in hardness with almost double the hardness increment. The low age hardening for the binary alloy was caused by the coarse

CHAMINI L. MENDIS, Post Doctoral Researcher, and KAZUHIRO HONO, Manager of Magnetic Materials Unit, are with the National Institute for Materials Science, Tsukuba 305-0047, Japan. Contact e-mail: mendis.chamini@nims.go.jp KEIICHIRO OH-ISHI, formerly with the National Institute for Materials Science, is now Adjunct Associate Professor, with Nagaoka University of Technology, Nagaoka 940-2188, Japan.

Manuscript submitted June 27, 2011.
Article published online January 20, 2012

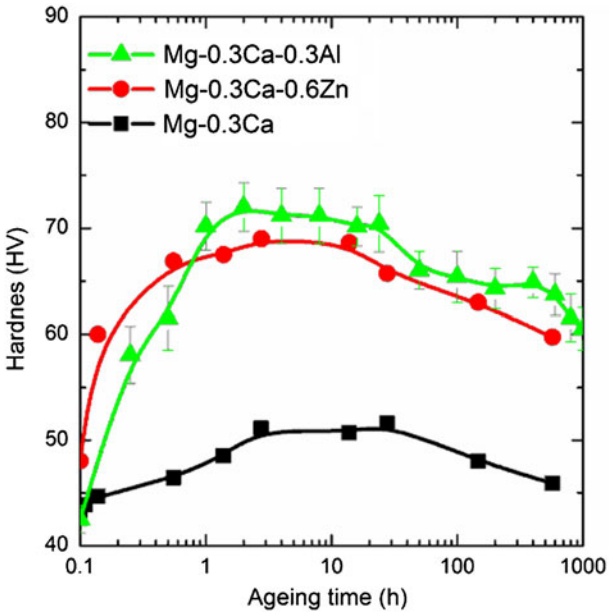

Fig. 1—Age-hardening responses of Mg-0.3Ca-0.6Zn[8] and Mg-0.3Ca-0.3Al[9] alloys compared with the Mg-0.3Ca[8] alloy at 473 K (200 °C) following solution treatment at 798 K (525 °C).

precipitation of the equilibrium Mg_2Ca phase as shown in Figure 2(a).[8] The structure of the Mg_2Ca phase is hexagonal with the lattice parameter of $a = 0.625$ nm and $c = 1.014$ nm, so the lattice mismatch with the Mg matrix is rather large. In contrast, a high number density of thin coherent plates with an average diameter of ~20 nm uniformly precipitated in the peak-aged Mg-0.3Ca-0.6Zn alloy, as shown in Figure 2(b). The microalloying of Al into Mg-Zn shows a similar enhancement of the age-hardening response, and the bright-field image of the peak-aged Mg-0.3Ca-0.3Al (Figure 2(c)) also shows a high number density of plate-like precipitates on the basal planes.[9] The diffraction patterns from the $[10\bar{1}0]_{Mg}$ zone showed that additional reflections are parallel to the $[11\bar{2}0]_{Mg}$ planes of Mg at one-third and two-thirds distance from the $[11\bar{2}0]_{Mg}$ reflection (the diffraction pattern is reported in Reference 9). Additionally the three-dimensional atom probe (3DAP) data also showed the presence of Al- and Ca-rich Guinier–Preston (GP) zones forming parallel to the $(0001)_{Mg}$ planes of magnesium as illustrated in Reference 9. These plate-like precipitates are similar to those reported by Suzuki as MgAlCa plates in the die-cast Mg-5Al-1Ca-0.05Sr (at. pct) (AXJ530 alloy).[10]

The high-angle annular dark field (HAADF) scanning transmission electron microscopy (STEM) images taken from the $[10\bar{1}0]_{Mg}$ zone show that these plates have only a single atomic layer thickness as shown in Figure 3(a). In addition, brightly imaged atomic columns are observed every two atomic columns along the $[11\bar{2}0]_{Mg}$ direction, suggesting that the position of Zn atoms are internally ordered within the (0001) plane so that Zn and Ca atoms can be neighbored. In contrast, the atomic columns observed along the $[11\bar{2}0]_{Mg}$ zone show uniform contrast. The $[11\bar{2}0]$ zone-diffraction

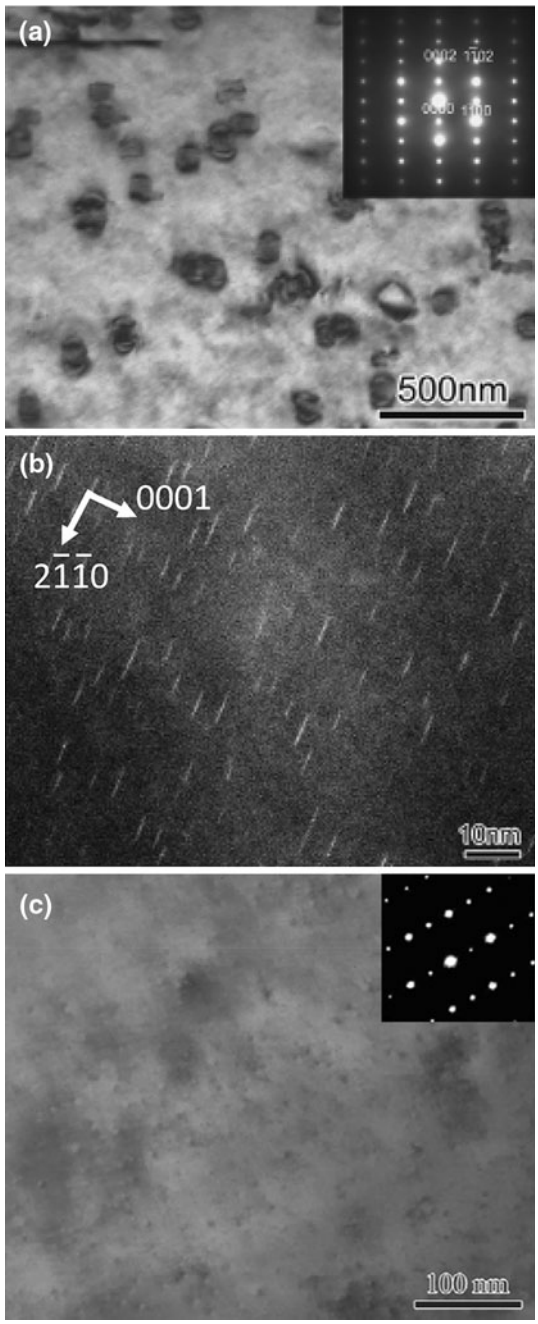

Fig. 2—The peak-aged microstructures of (*a*) Mg-0.3Ca,[8] (*b*) Mg-0.3Ca-0.6Zn,[8] and (*c*) Mg-0.3Ca-0.3Al[9] alloys. The electron beam parallel to (a) and (c) $\langle 11\bar{2}0\rangle_{Mg}$ and parallel to (b) $\langle 10\bar{1}0\rangle_{Mg}$.

pattern recorded from the peak-aged alloy shows streaks parallel to the $[0001]_{Mg}$ direction. On the $\langle 10\bar{1}0\rangle_{Mg}$ zone axis pattern, in addition to the streaks parallel to the $\{11\bar{2}0\}_{Mg}$ planes, streaks were present at one-third and two-thirds distance from the $\{11\bar{2}0\}_{Mg}$ planes (Figures 3(c) and (d)). Because the plate-like precipitates have the same structure as the matrix phase, with only a difference in chemistry, they can be defined as internally ordered GP zones. The plate-like precipitates in the Mg-Ca-Al alloy also had the same structure (*i.e.*, internally ordered single-layer GP zones).[9][8]

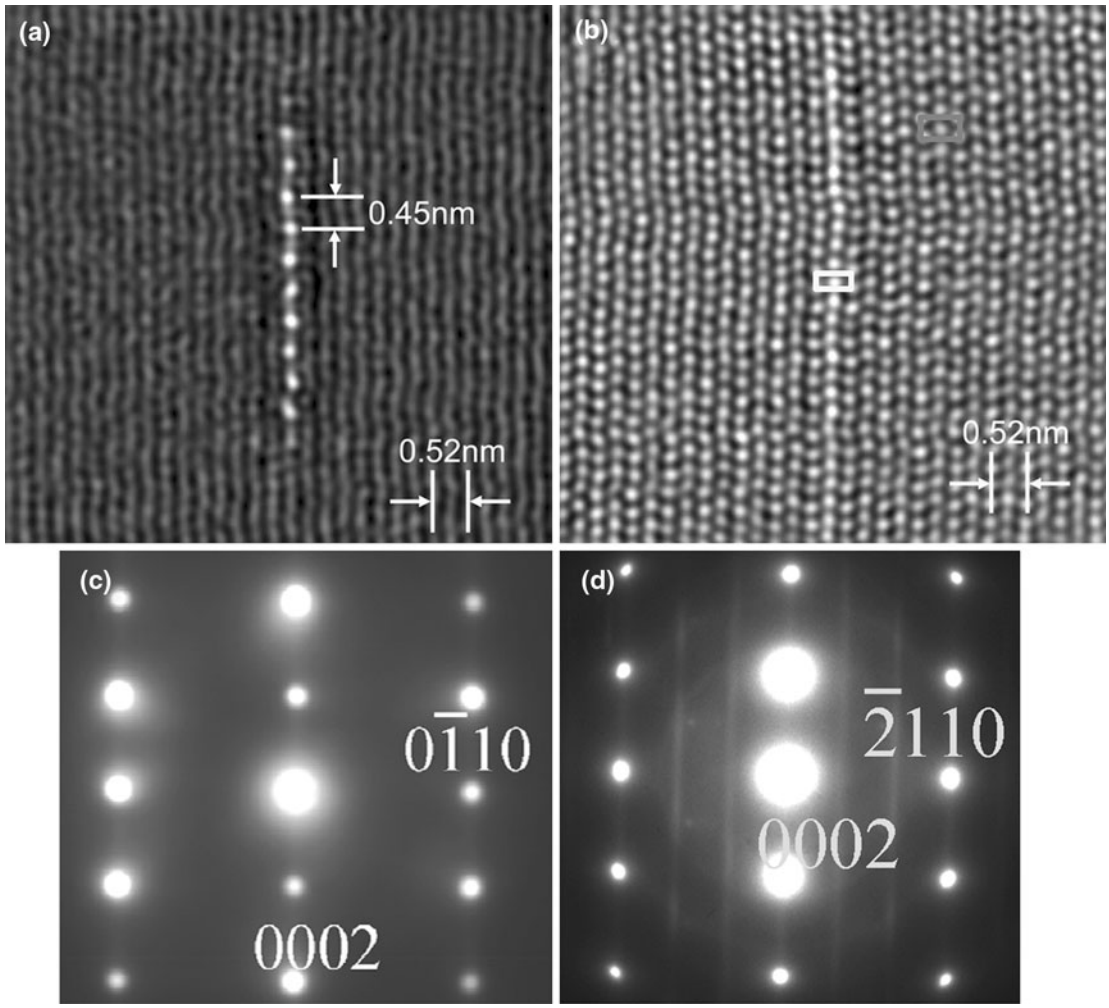

Fig. 3—The HAADF-STEM micrographs showing the GP zones observed in Mg-0.3Ca-0.6Zn alloy at maximum hardness with the electron beam parallel to (*a*) $\langle 11\bar{2}0\rangle_{Mg}$ and (*b*) $\langle 10\bar{1}0\rangle_{Mg}$. The corresponding selected area diffraction patterns (*c*) $\langle 11\bar{2}0\rangle_{Mg}$ and (*d*) $\langle 10\bar{1}0\rangle_{Mg}$.[8]

III. PRISMATIC PLATES IN MG-CA ALLOY MICROALLOYED WITH IN

Nie[11] reported that basal precipitates are not so effective in age hardening compared with the prismatic plates because dislocations gliding on the basal planes easily bypass the basal plates. The precipitation hardening depends on the inter-particle distance. For a given volume fraction and number density of precipitates, the effectiveness of the precipitates depends on the shape and orientation of the particles. The effectiveness of precipitation hardening decreases in the order of prismatic/pyramidal plates, $[0001]_{Mg}$ rods, spherical precipitates, and basal plates or laths. To obtain more effective precipitation hardening, platelets on prismatic or pyramidal planes are desirable. This process has been experimentally demonstrated in WE54 (Mg-5wt pct Y-4wt pct RE) alloy where significantly high precipitation hardening is caused by the formation of prismatic plates.[12,13] Other than the Mg-Y-RE system, Sasaki *et al*. reported that prismatic plates can be formed in Mg-Bi-Zn alloys,[14] but their number density and aspect ratio are not high enough. Because the precipitate

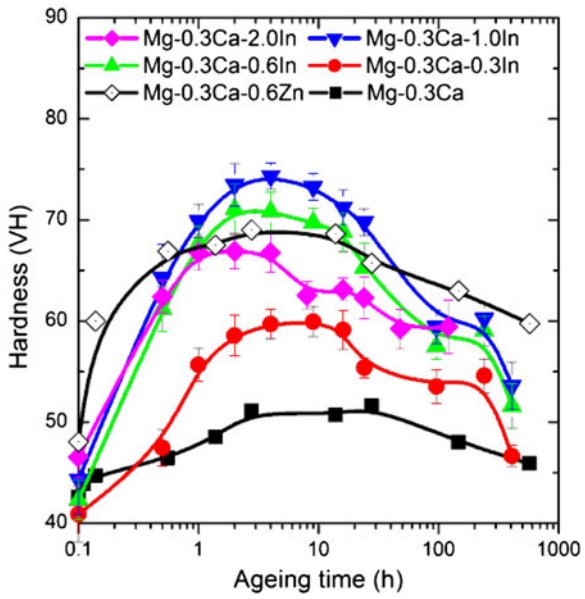

Fig. 4—Age-hardening response of Mg-0.3Ca-(0-2)In[19] alloys compared with the Mg-0.3Ca-0.6Zn[8] alloy.

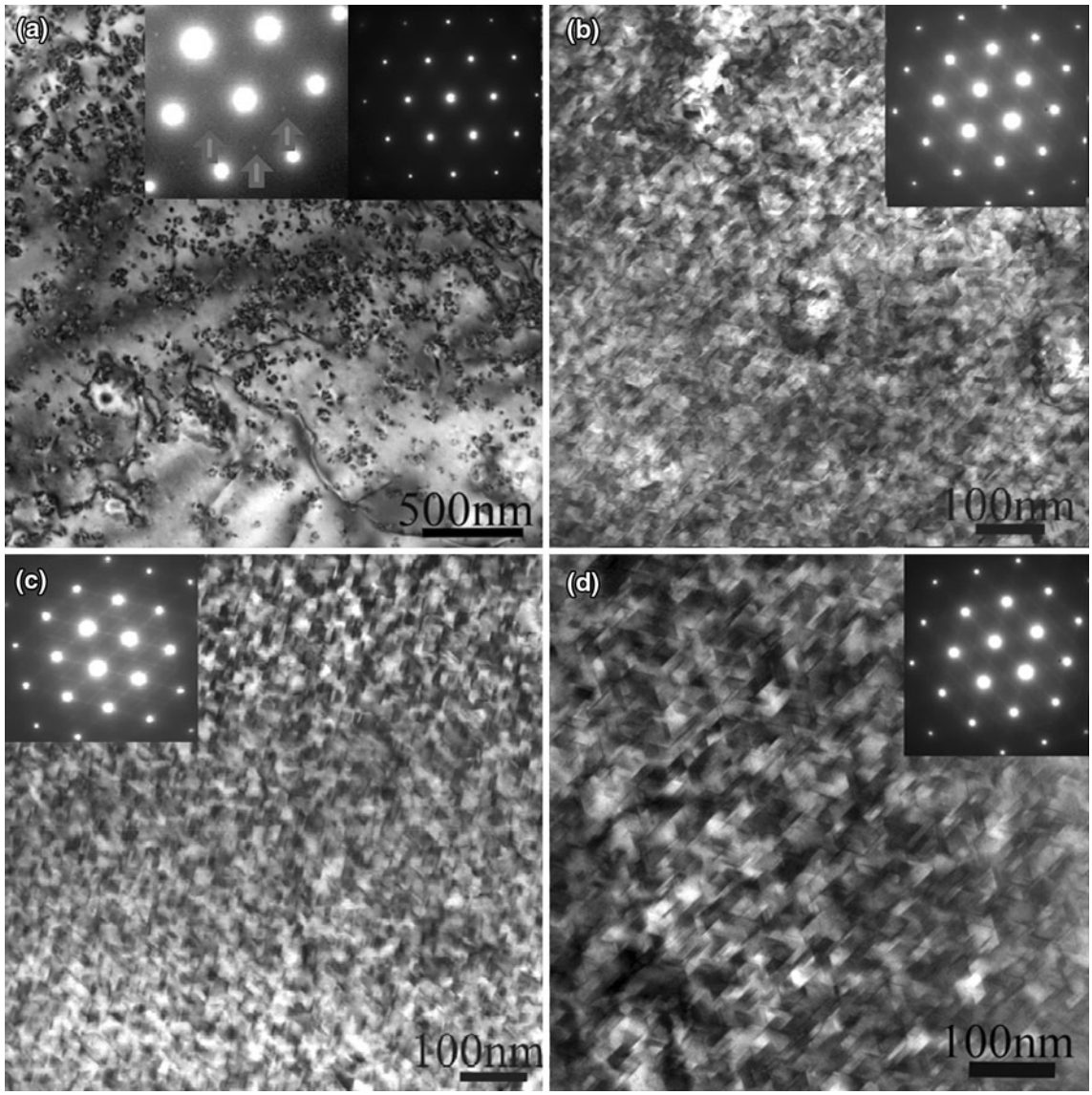

Fig. 5—The microstructures of peak-aged Mg-0.3Ca-(0.3-2)In[19] alloys. The electron beam parallel to $[0001]_{Mg}$. (*a*) Mg-0.3Ca-0.3In, (*b*) Mg-0.3Ca-0.6In, (*c*) Mg-0.3Ca-1.0In, and (*d*) Mg-0.3Ca-2In alloys.

morphology is determined by the strain field, adjusting the atomic size of the atoms that co-cluster with the major alloying element may alter the habit plane of the metastable precipitates. Based on this idea, we tested indium (In) as a microalloying element, whose atomic radius is nearly the same as that of Mg.

The age-hardening response of the Mg-0.3Ca alloys microalloyed with In is shown in Figure 4 along with that of the Mg-0.3Ca-0.6Zn alloy.[6] The hardness values of the as-quenched Mg-0.3Ca-(0.3-2)In alloys are all ~45 VH comparable with the binary alloy. The age-hardening response increases with In concentration up to 1 at. pct with the maximum hardness of 75 VH after 2 hours of aging with an increment of ~30 VH, which is higher than the peak hardness of the Mg-0.3Ca-0.6Zn alloy. Continued increase in the In concentration decreases the peak hardness.

The transmission electron microscopy (TEM) bright-field images of the peak-aged Mg-0.3Ca-(0.3-2)In alloys are shown in Figure 5 with an electron beam parallel to the $[0001]_{Mg}$ zone axis. The low-magnification images of the Mg-0.3Ca-0.3In alloy show large cuboidal particles of ~50 nm uniformly distributed though the microstructure, which is the equilibrium Mg_2Ca phase, as illustrated by the enlarged diffraction pattern inserted in Figure 5(a). The extra reflections are a result of the presence of Mg_2Ca with the orientation relationship described by Nie and Muddle.[15] However, at a higher magnification, plate-like precipitates are also observed in the matrix. These plate-like precipitates can be more clearly observed in the alloy with In higher than 0.6 at. pct with no cuboidal precipitates. The number density of the plate-like precipitates is the largest in the Mg-0.3Ca-1.0In alloy.

The plate-like precipitates in the peak-aged Mg-0.3Ca-1.0In alloy is shown with a higher magnification in Figure 6. The plates are on the $\{10\bar{1}0\}_{Mg}$ prismatic planes. In average, the particle size is 20 ± 2.5 nm in

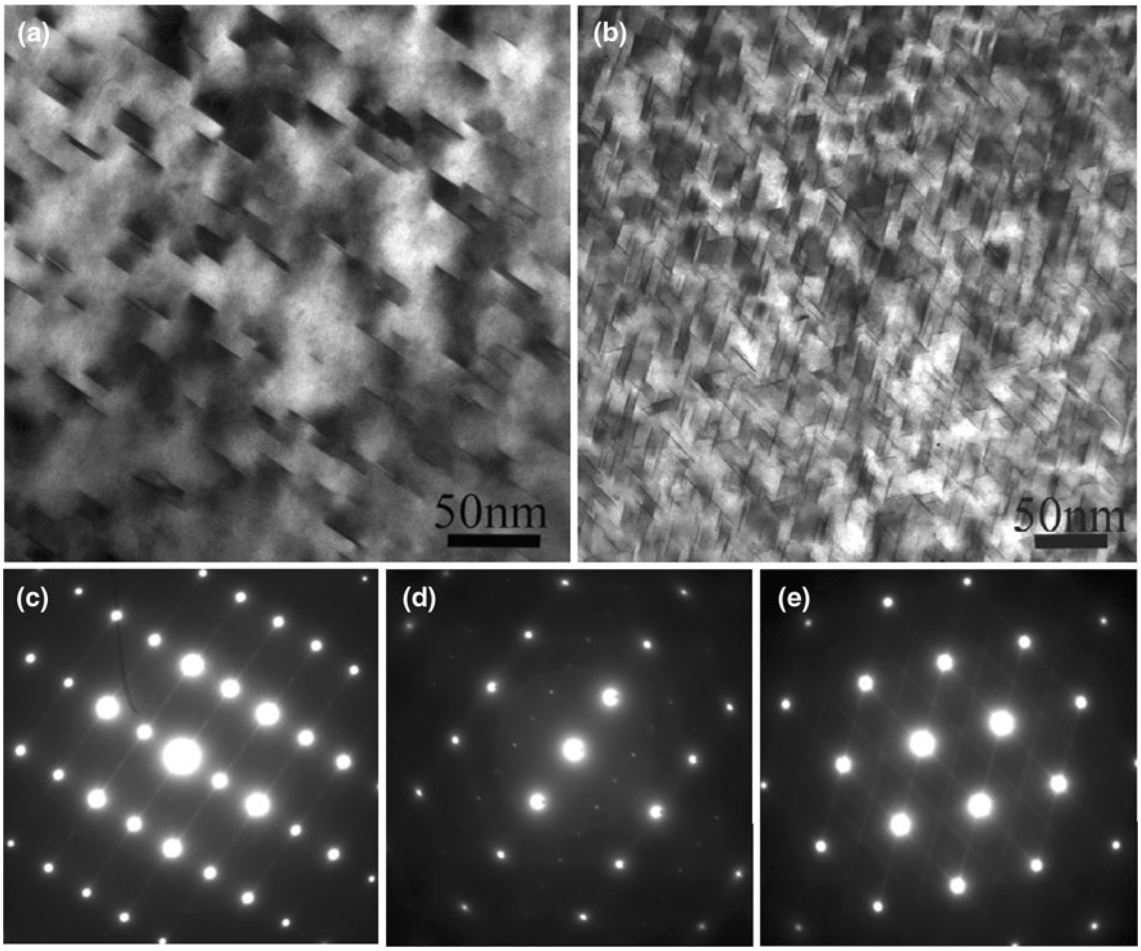

Fig. 6—The TEM micrographs of Mg-0.3Ca-1.0In[19] alloy aged to (*a*) and (*b*) peak hardness (2 h at 473 K [200 °C]). Electron beam is parallel to (*a*) $\langle 11\bar{2}0 \rangle$ and (*b*) [0001]. The selected area diffraction patterns recorded are parallel to (*c*) $\langle 11\bar{2}0 \rangle$, (*d*) $\langle 10\bar{1}0 \rangle$, and (*e*) [0001] zone axis of magnesium.

diameter. The thickness of these precipitates cannot be determined accurately from the TEM bright-field images because of the large strain contrast near the plates. The diffraction patterns from the $[0001]_{Mg}$ zone axis show streaks parallel to $\{11\bar{2}0\}_{Mg}$ and spots at one-quarter, one-half, and three-quarters distance from the $\{11\bar{2}0\}_{Mg}$ diffraction spots. The $\langle 11\bar{2}0 \rangle_{Mg}$ zone axis shows streaks parallel to the (0001) diffraction spots. However, no streaks are observed on the $\langle 10\bar{1}0 \rangle_{Mg}$ zone, but diffraction spots are observed as the Ewald sphere cut through the streaks forming parallel to the zone. The streaks do not show intensity maxima associated with the periodic structure in the normal direction to the plane; thus, the plates are iso-structure with a hexagonal close-packed Mg matrix.

Figure 7 shows TEM bright-field images of the Mg-0.3Ca-0.3In alloy over-aged for 240 hours at 473 K (200 °C). The cuboidal-shaped precipitates have been identified as the equilibrium Mg_2Ca phase. The Mg-0.3Ca-0.6In and Mg-0.3Ca-1.0In samples also contain cuboidal particles distributed in a non-uniform manner. A diffraction pattern typical of those recorded from the $\langle 11\bar{2}0 \rangle_{Mg}$ zone from an area containing coarse precipitates in all three alloys is shown in Figure 8(d) and is indexed according to Mg_2Ca phase and is consistent with the orientation relationship described by Nie and Muddle.[15] At higher magnifications, the plate-like precipitates are also observed between the cuboidal particles as shown in Figures 8(a) and (b). The prismatic plates are approximately 200 ± 43 nm in diameter and the thickness of these plates remains ~0.5 ± 0.1 nm. The aspect ratio of these precipitates is ~133. The selected area diffraction patterns taken from the regions containing the prismatic plates are comparable with those in the peak-aged alloys, suggesting that the structure of the plate-like precipitates remains the same even in the over-aged condition.

The HAADF–STEM images of the Mg-0.3Ca-1.0In alloy in the peak-aged condition are shown in Figure 9. The number density of the prismatic plates was estimated to be ~3.2×10^{22} m^{-3}, which is comparable with the number density of the θ' precipitates in the peak-aged Al-1.7 at. pct Cu alloy (base composition for A2014). Higher magnification HAADF-STEM reveals that the GP zones are two atomic layers thick consisting of both Ca and In. Based on the brightness of the HAADF image, we infer the precipitate has an In layer followed by Ca atom layers, leading to a zigzag arrangement of the In and Ca atoms as shown in Figure 9(c). A magnesium unit cell drawn away from the GP zone in Figure 9(b) has

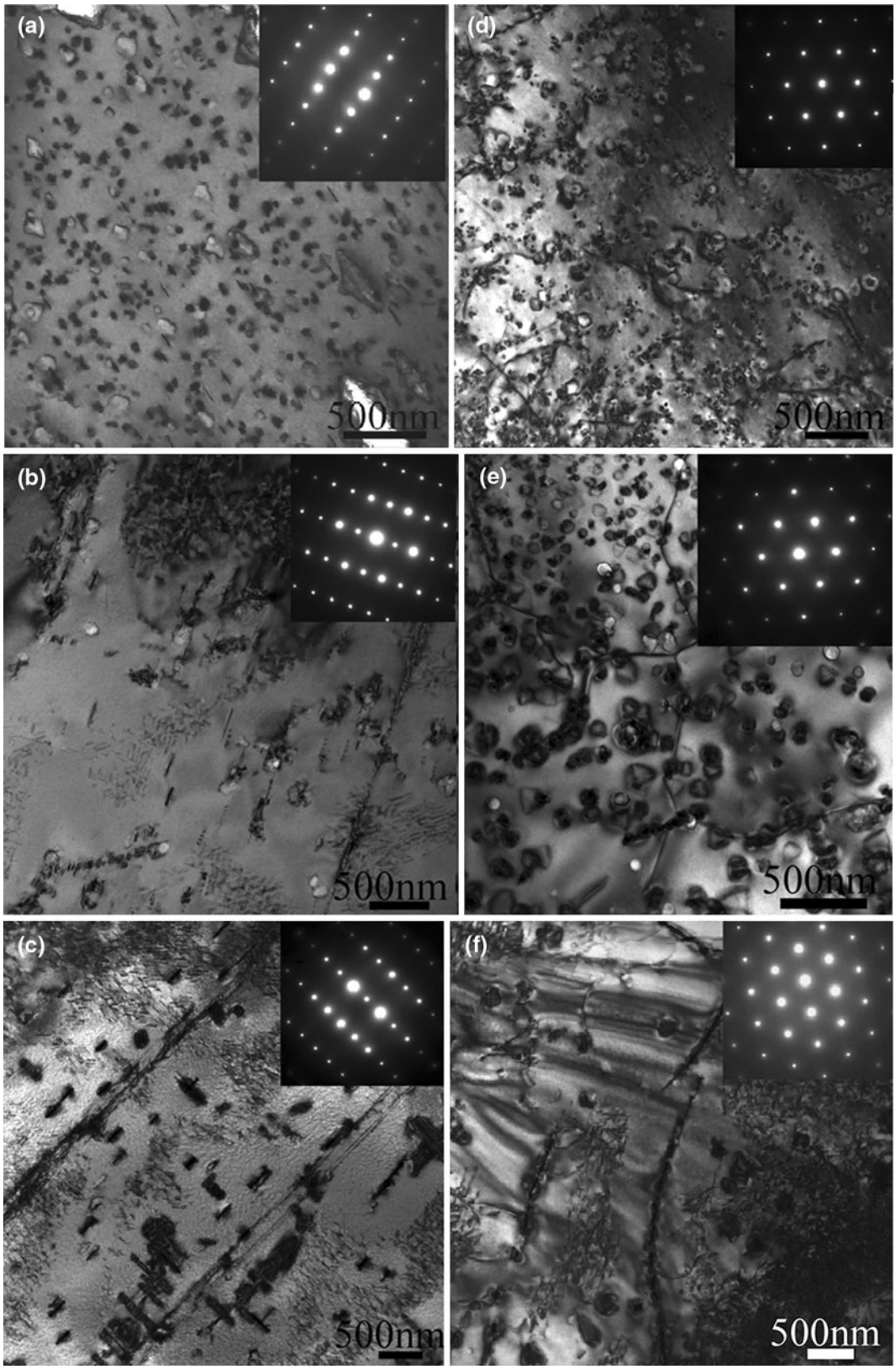

Fig. 7—The TEM bright-field images of the Mg-0.3Ca-(0.3-2)In alloys overaged for 240 h at 473 K (200 °C). The electron beam parallel to (*a*) through (*c*) $\langle 11\bar{2}0 \rangle_{Mg}$ and parallel to (*d*) through (*f*) $[0001]_{Mg}$. (a) and (d) Mg-0.3Ca-0.3In, (b) and (e) Mg-0.3Ca-0.6In, and (c) and (f) Mg-0.3Ca-1.0In alloys.

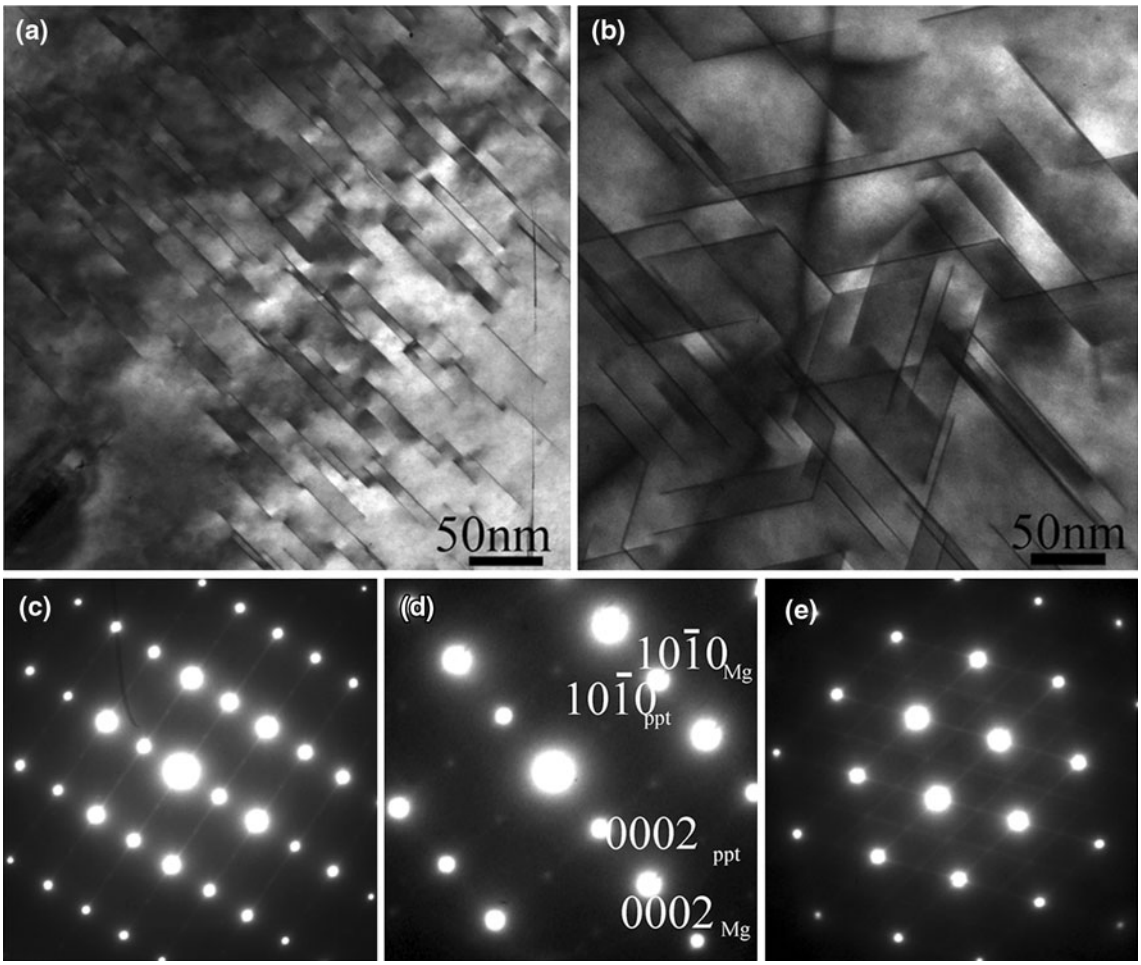

Fig. 8—The TEM micrographs of Mg-0.3Ca-1.0In alloy aged for 240 h at 473 K (200 °C) showing regions with prismatic plate GP zones. The electron beam is parallel to (*a*) $\langle 11\bar{2}0 \rangle$ and (*b*) [0001]. The selected area diffraction patterns recorded parallel to (*c*) and (*d*) $\langle 11\bar{2}0 \rangle$, and parallel to (*e*) the [0001] zone axis of magnesium. Diffraction patterns from (d) is from an area containing coarse Mg_2Ca particles.

dimensions of 0.514 nm in height and 0.275 nm in width (shown in red and marked 1). This distance is equivalent to the distance between $(0001)_{Mg}$ and $\{10\bar{1}0\}_{Mg}$ planes of Mg 0.514 nm and 0.277 nm, respectively, and is the height and width of the unit cell. A similar unit cell (shown in yellow and marked 2) is drawn over the GP zones, which shows that the height of the cell remains 0.514 nm, whereas the width of the unit cell is ~0.34 nm along $[0001]_{Mg}$ and $\langle 10\bar{1}0 \rangle_{Mg}$ directions, respectively. The unit cell thus created is ~23 pct larger in the $\langle 10\bar{1}0 \rangle_{Mg}$ direction, whereas no difference is detected parallel to the $[0001]_{Mg}$ direction. A unit cell drawn in the Mg matrix close to the GP zones (shown in Green and marked 3) shows that the width of the unit cell (distance between $\{10\bar{1}0\}_{Mg}$ planes) is ~0.245 nm, which is ~11 pct smaller than a similar distance measured away from the GP zones. It does not seem to impose any strain in the GP zones alone the $[0001]_{Mg}$ directions, but it will cause a coherent compressive strain parallel to the $\langle 10\bar{1}0 \rangle_{Mg}$ directions.

The atom probe tomography showing Ca and In atoms in the peak-aged Mg-0.3Ca-1.0In alloy is shown in Figure 10 together with the concentration depth profile calculated from the inset box. The three variants of Ca-In enriched plates are observed. The composition of these plates is approximately 7.5 at. pct Ca and 4.0 at. pct In. Because of the thinness of the precipitates, it is likely that the Mg atoms from the matrix were also detected from the precipitates, so the actual solute concentration in the precipitates should be higher than the measured values. The number density of the prismatic GP zones calculated from the atom probe data is 5×10^{22} m^{-3}, which is consistent with the values calculated from the HAADF data shown previously. The atom probe data was also collected from the over-aged Mg-0.3Ca-1.0In alloy in the regions where prismatic plate GP zones were prevalent (Figure 11). Again three different variants of GP zones are observed. The composition of the GP zones is approximately 8.3 at. pct Ca and 3.1 at. pct In. The In composition of the GP zones is lower than that observed for the peak-aged alloy.

IV. DISCUSSION

In both Mg-RE-X and Mg-Ca-X alloys, where RE stands for rare earth elements and X is Zn and Al, the

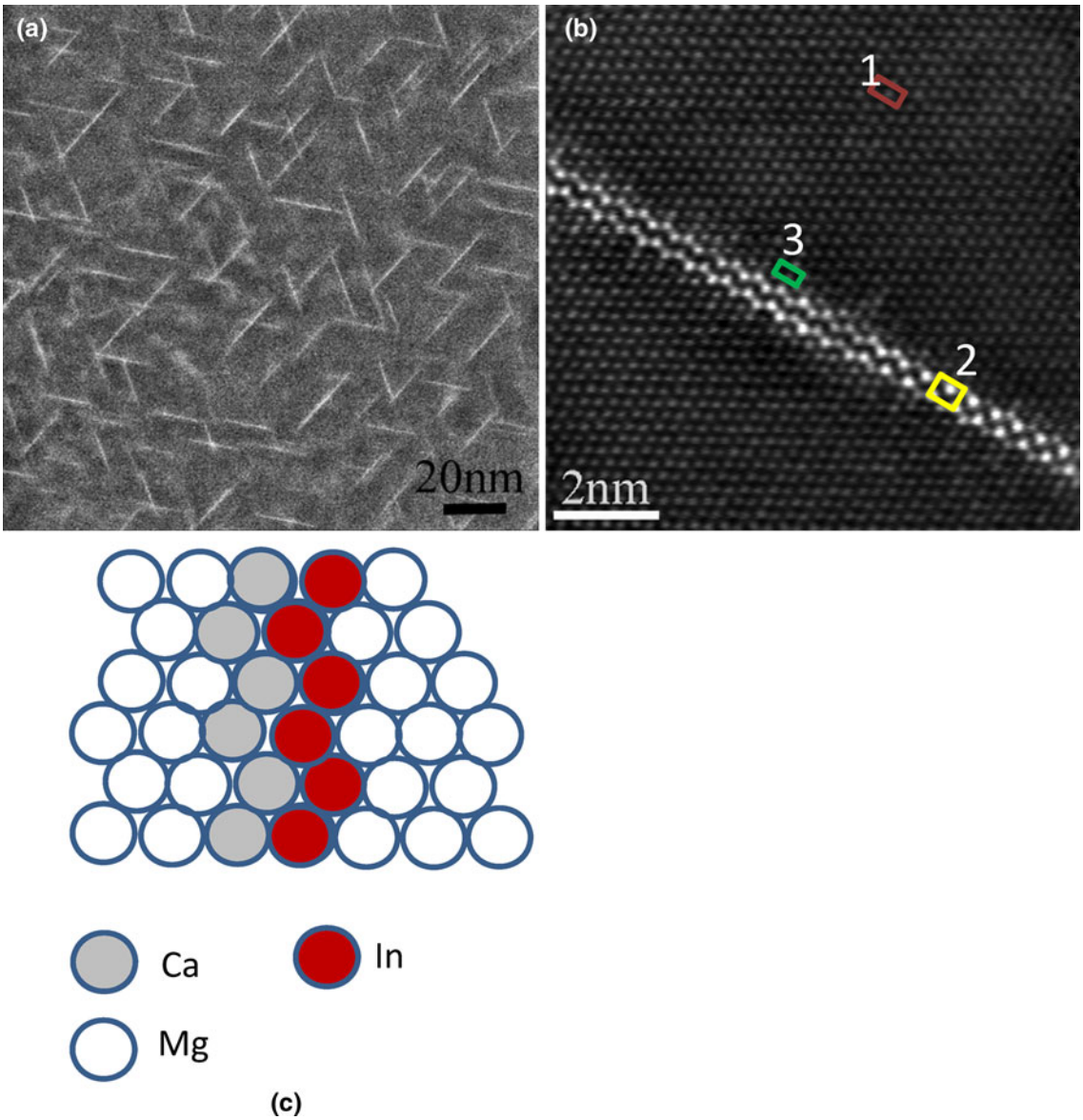

Fig. 9—HAADF-STEM images of Mg-0.3Ca-1.0In alloy aged to peak hardness with an electron beam parallel to (*a*) [0001] and (*b*) $\langle 11\bar{2}0 \rangle$. (*c*) Schematic showing the arrangement of Ca and In atoms in GP zones parallel to $\langle 11\bar{2}0 \rangle$ (Color figure online).

plate-like precipitates are formed, but they are all on the basal plane. The uniform dispersion of the fine prismatic plates observed in the Mg-0.3Ca-1.0In alloys is the first case with the exception of WE54 (Mg-1.2Y-0.5RE [at. pct]) where $Mg_{14}Nd_2Y$ intermediate phase was observed.[12,13] In the WE54 alloy, the number density of the precipitates is only in the order of 10^{19} m^{-3}, and the aspect ratio of the precipitates is ~10 with a coarse size.[13] The aspect ratio of the GP zones in the peak-aged Mg-0.3Ca-1.0In alloy is ~67. This ratio is substantially higher than that observed for the WE54 alloy in the peak-aged condition. A higher aspect ratio of 133 was observed in the over-aged Mg-0.3Ca-1.0In alloy, but because of the heterogeneous distribution of these precipitates, it does not result in a high hardness value. The minor addition of Zn was reported to alter the habit planes of the precipitates in the Mg-Sn[16,17] and Mg-Bi[14] systems, but only a minor volume fraction of precipitates changes the habit plane from the basal to prismatic type in these cases. In the Mg-0.3Ca-1.0In alloy, the complete transformation to prismatic GP zones was observed.

The minor addition of Zn and Al to the Mg-0.3Ca system leads to the formation of plate-like GP zones on the basal plane. Zn and Al atoms both have a smaller atomic radius compared with Mg, whereas Ca has a larger atomic radius. In contrast, the atomic radius of In is nearly the same as that of Mg. The Zn, Al, and In all have negative enthalpies when mixed with Ca; thus they tend to co-segregate with Ca when Ca precipitates out from the Mg matrix. The atomic arrangement of the GP zones in the Mg-0.3Ca-0.6Zn and Mg-0.3Ca-0.3Al alloys based on the HAADF results indicates that Ca atoms are the next to the smaller diameter atoms, Al and Zn. The presence of Ca atoms next to Zn atoms reduces the strain imposed on the Mg matrix on the basal planes. A similar

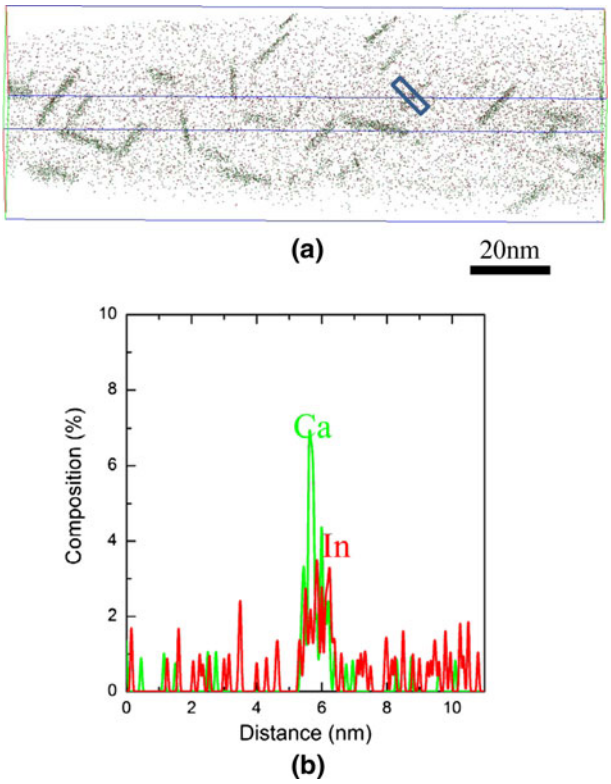

Fig. 10—3DAP tomography results for the Mg-0.3Ca-1.0In alloy aged to peak hardness (2 h at 473 K [200 °C]) (*a*) from the volume investigated, and (*b*) composition profile from the particle boxed in (a).[19]

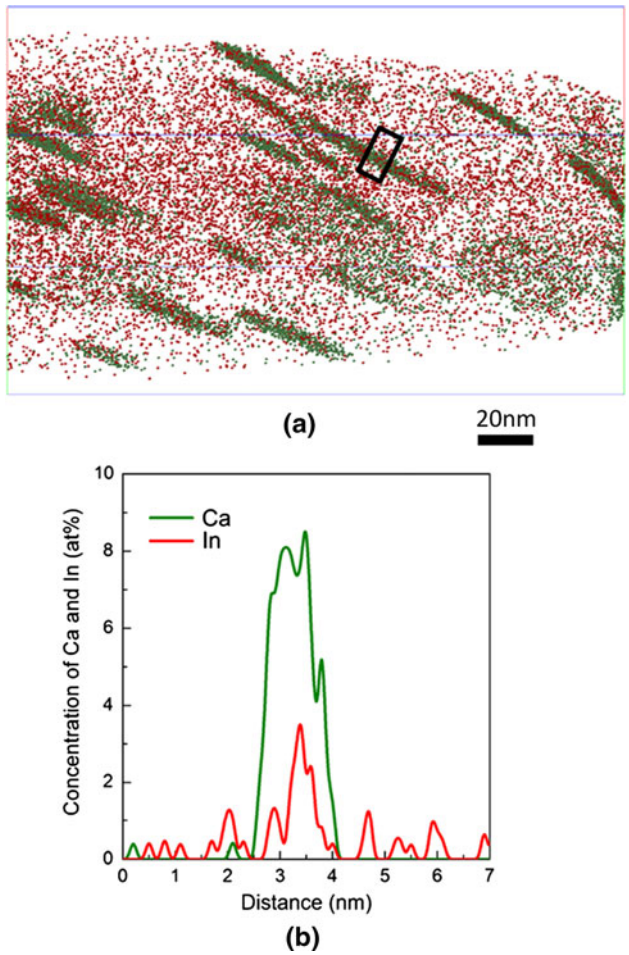

Fig. 11—3DAP tomography results for the Mg-0.3Ca-1.0In alloy aged for 240 h at 473 K (200 °C) (overaged) (*a*) from the volume investigated, and (*b*) composition profile from the particle boxed in (a).

arrangement of Ca and In atoms will not lead to the reduction of strain on the basal plane as both elements have a larger atomic size compared with Mg.

Based on Figure 9(b), the compressive strain imposed on the matrix resulting from the formation of the prismatic plate can be estimated to be ~9 pct along the $\langle 10\bar{1}0 \rangle_{Mg}$ direction. A similar calculation can be made for the Mg-0.3Ca-0.6Zn alloy based on the data by Oh-ishi *et al.*[8] The unit cell drawn away from the GP zone (shown in red and marked 1 in Figure 3) shows a height of 0.52 nm and a width of 0.28 nm, which are equivalent to the distance between $(0001)_{Mg}$ and $\{10\bar{1}0\}_{Mg}$ planes in Mg. The unit cell drawn similarly over the GP zone shows a height of 0.52 nm and a width of 0.24 nm along the $[0001]_{Mg}$ and $\langle 10\bar{1}0 \rangle_{Mg}$ directions (drawn in yellow and marked 2). The unit cell thus created is ~14 pct smaller in the $\langle 10\bar{1}0 \rangle_{Mg}$ direction, whereas no difference is detected parallel to the $[0001]_{Mg}$ direction. The third unit cell cannot be drawn in this case, but a simple calculation suggests that a tensile strain of ~7 pct is imposed on the matrix adjacent to the ends of the GP zones. The strain measured from the HAADF-STEM image of the Mg-0.3Ca-0.6Zn alloy was similar to the strain calculated assuming that Ca atom and Zn atoms are in adjacent atomic positions on the basal plane. However, having Ca and In atoms in the adjacent atomic positions on the basal plane would result in a much larger strain. The placement of Ca and In atoms as illustrated in Figure 9(b) in a zigzag manner reduces the calculated value of strain imposed on the matrix. The reasons behind the formation of prismatic and basal precipitates in this case may be understood according to the reduction of the misfit strain energy associated with accommodating the GP zones in prismatic or basal planes.

In the Mg-0.3Ca-1.0In alloy, no driving force exists for the In atom to precipitate out as the solid solubility of In in Mg as ~12 at. pct at temperatures below 773 K (500 °C),[4] suggesting that In can form solid solution with Mg. In contrast, because Ca has little solubility in Mg, Ca precipitates during aging. Because In has a high negative enthalpy when mixed with Ca, In atoms segregate with Ca. Initially, Ca and In atoms cocluster, and the morphology changes to the prismatic plate to reduce the strain energy as the cluster size increases. In the over-aged condition, the equilibrium Mg_2Ca phase precipitates at the expense of GP zones as illustrated by Figures 7(c) and (d).

Based on the 3DAP results, the number density of the GP zones were estimated to be ~4.96×10^{22} m^{-3} in the peak-aged condition, which results in a hardening increment of ~30 VH. The number density of the atom probe data is in the same order. The age-hardening increment of the Mg-0.3Ca-0.3Al alloy was ~27 VH at

200 °C at the peak hardness condition,[9] in which the number density of the basal plate GP zone was ~$7.2 \times 10^{24} m^{-3}$,[9] which is two orders magnitude higher than that in the Mg-0.3Ca-1.0In alloy. This indicates that the prismatic GP zones are much more effective for the hardness increase despite the lower number density. This suggests that prismatic plates are more effective in hindering the motion of dislocations than basal plates.

V. CONCLUDING REMARKS

The age-hardening response of Mg-Ca alloy can be substantially enhanced by the microalloying with Al, Zn, and In. These cause the formation of metastable plate-like internally ordered GP zones in the peak-aged condition, which are uniformly dispersed in the matrix with relatively good thermal stability. The plate-like GP zones observed in the Mg-Ca-Zn and Mg-Ca-Al alloys are fully coherent single-layer precipitates with an atomic order within the layer. This ordered structure is considered to be a result of the negative enthalpy of mixing between Ca and Zn and their paring compensation of the misfit. The addition of In alters the habit plane to the prismatic plane, which is expected to be a more effective barrier for the dislocation movement. Like Al and Zn, the enthalpy of mixing between Ca and In is negative, but the atomic radius of In is similar to that of Mg. Hence, we believe that the basal plate morphology of the Ca-In GP zones leads to lower misfit strain with the matrix.

The plate-like GP zones in Mg-Ca-Al has been proposed to be effective in improving the creep resistance of the alloy,[18] and the combination of age hardening and improved creep resistance may lead to the development of new wrought Mg-Ca alloys using Zn or Al. Because In is expensive, it will be industrially unviable, but the elucidation of the mechanism of the habit plane control may lead to alloy developments with a higher age-hardening response with prismatic plates.

ACKNOWLEDGMENTS

This work was in part supported by the Grant-in-Aid for Scientific Research (B), 21360348, 2009, and by World Premier International Research Center for Materials Nanoarchitectonics, MEXT. The 3DAP work was supported by CREST-JST. This work was also partially supported by the Fundamental R&D Program for Core Technology of Materials funded by the Ministry of Industry, Trade and Energy, Center for Nanostructured Materials Technology under the 21st Century Frontier R&D Programs of the Ministry of Science and Technology, Korea through the Korea Institute of Science and Technology.

REFERENCES

1. K. Hono, C.L. Mendis, K. Oh-ishi, and T.T. Sasaki: *Scripta Mater*., 2010, vol. 63, pp. 710–15.
2. C.L. Mendis, K. Oh-ishi, and K. Hono: *Scripta Mater*., 2007, vol. 59, pp. 485–88.
3. C.L. Mendis, K. Oh-ishi, Y. Kawamura, T. Honma, S. Kamado, and K. Hono: *Acta Mater*., 2009, vol. 57, pp. 749–60.
4. C.L. Mendis, J.H. Bae, N.J. Kim, and K. Hono: *Scripta Mater*., 2011, vol. 64, pp. 335–38.
5. T.T. Sasaki, K. Yamamoto, T. Honma, S. Kamado, and K. Hono: *Scripta Mater*., 2008, vol. 59, pp. 1111–14.
6. A.A. Nayeb-Hashemi and J.B. Clark, .: *Phase Diagrams of Binary Magnesium Alloys*, ASM International, Materials Park, OH, 1988.
7. X. Gao, S.M. Zhu, B.C. Muddle, and J.F. Nie: *Scripta Mater*., 2005, vol. 53, pp. 1321–26.
8. K. Oh-ishi, R. Watanabe, C.L. Mendis, and K. Hono: *Mater. Sci. Eng. A*, 2009, vol. 526, pp. 177–84.
9. J. Jayaraj, C.L. Mendis, K. Oh-ishi, T. Ohkubo, and K. Hono: *Scripta Mater*., 2010, vol. 63, pp. 831–34.
10. A. Suzuki, N.D. Saddock, J.R. Terbush, B.R. Powell, J.W. Jones, and T.M. Pollock: *Metall. Mater. Trans. A*, 2008, vol. 39A, pp. 696–702.
11. J.F. Nie: *Scripta Mater*., 2001, vol. 48, pp. 1009–15.
12. G.W. Lorimer, R.A. Khosroshahi, and M. Ahmed: in *Int. Conf. on Solid-Solid Phase Transformations '99 (JIMIC -3)*, M. Koiwa, K. Otsuka, T. Mitazaki, eds., 1999, vol. 12, pp. 185–92.
13. J.F. Nie and B.C. Muddle: *Acta Mater*., 2000, vol. 48, pp. 1691–703.
14. T.T. Sasaki, T. Ohkubo, and K. Hono: *Scripta Mater*., 2009, vol. 61, pp. 72–75.
15. J.F. Nie and B.C. Muddle: *Scripta Mater*., 1997, vol. 37, pp. 1475–81.
16. T.T. Sasaki, K. Oh-ishi, T. Ohkubo, and K. Hono: *Scripta Mater*., 2006, vol. 53, pp. 251–54.
17. C.L. Mendis, C.J. Bettles, M.A. Gibson, and C.R. Hutchinson: *Mater. Sci. Eng. A*, 2006, vols. 435–436, pp. 163–71.
18. T. Homma, S. Nakawaki, and S. Kamado: *Scripta Mater*., 2010, vol. 63, pp. 1173–76.
19. C.L. Mendis, K. Oh-ishi, T. Ohkubo, and K. Hono: *Scripta Mater*., 2011, vol. 64, pp. 137–40.